Dual band HEIWIP detectors with nitride materials

A. G. Unil Perera[a], Gamini Ariyawansa[a], Ranga Jayasinghe[a], Laura Byrum[a], Nikolaus Dietz[a], Steven G. Matsik[b], Ian T. Ferguson[c], Hui Luo[d], Andrew Bezinger[d], and Hui Chun Liu[d]

[a]Department of Physics and Astronomy, Georgia State University, Atlanta, Georgia 30303, USA;
[b]NDP Optronics LLC, Mableton, Georgia 30126, USA;
[c]School of Electrical and Engineering, Georgia Institute of Technology, Atlanta, Georgia 30332, USA:
[d]Institute for Microstructural Sciences, National Research Council, Ottawa K1A OR6, Canada

ABSTRACT

Detection of both UV and IR radiation is useful for numerous applications such as firefighting and military sensing. At present, UV and IR dual wavelength band detection requires separate detector elements. Here results are presented for a GaN/AlGaN single detector element capable of measuring both UV and IR response. The initial detector used to prove the dualband concept consists of an undoped AlGaN barrier layer between two highly doped GaN emitter/contact layers. The UV response is due to interband absorption in the AlGaN barrier region producing electron-hole pairs which are then swept out of the barrier by an applied electric field and collected at the contacts. The IR response is due to free carrier absorption in the emitters and internal photoemission over the work function at the emitter barrier interface, followed by collection at the opposite contact. The UV threshold for the initial detector was 360 nm while the IR response was in the 8-14 micron range. Optimization of the detector to improve response in both spectral ranges will be discussed. Designs capable of distinguishing the simultaneously measured UV and IR by using three contacts and separate IR and UV active regions will be presented. The same approach can be used with other material combinations to cover additional wavelength ranges, e.g. GaAs/AlGaAs NIR-FIR dual band detectors.

Keywords: UV-IR dual band detector, GaN detector

1. INTRODUCTION

During the last decade, there has been an increased use of group III-Nitrides for electronic and optoelectronic devices including ultra-violet (UV) detectors,[1,2] UV light emitting diodes[3–5] and laser diodes.[6] These products are now commercially available for applications such as flame detection, UV imaging, solar UV detection, and military and industrial applications such as those focusing on agricultural and automotive products. Quantum well infrared photodetectors (QWIPs)[7] and GaN/AlGaN Schottky photodiodes,[8] operating in near-/mid-infrared (NIR/MIR) regions have been reported. Dual band detectors operating in the NIR and MIR/far-infrared (FIR) regions[9–11] based on the group III-As material system have been reported. Previously a detector responding in both the UV and MIR ranges was reported,[12] however, the detector needed separate modulation to distinguish UV and IR radiation. Here results are reported on a detector capable of operating in both the UV and 8-14 μm IR spectral ranges simultaneously without separately modulating the incident radiation, thus eliminating the difficulties of assembling several detectors when multiband detection is required. UV/IR dual-band detectors could be used in applications where the detection of both UV and IR radiation is important. In fire and flame detection, flames originating from different fuel materials, such as hydrogen and coal, have significant intensity variation in the emission spectrum in the UV and IR regions.

2. BASIC UV-IR DUAL BAND DETECTION

A simple structure for a UV-IR dual band detector with a non-intentionally doped AlGaN barrier between two highly doped GaN emitters is shown in Fig. 1. The basic dual band detection involves two different detection mechanisms to cover the separate ranges. The energy band diagram of a simple UV-IR detector with

Infrared Spaceborne Remote Sensing and Instrumentation XV, edited by Marija Strojnik-Scholl,
Proc. of SPIE Vol. 6678, 66780S, (2007) · 0277-786X/07/$18 · doi: 10.1117/12.734731

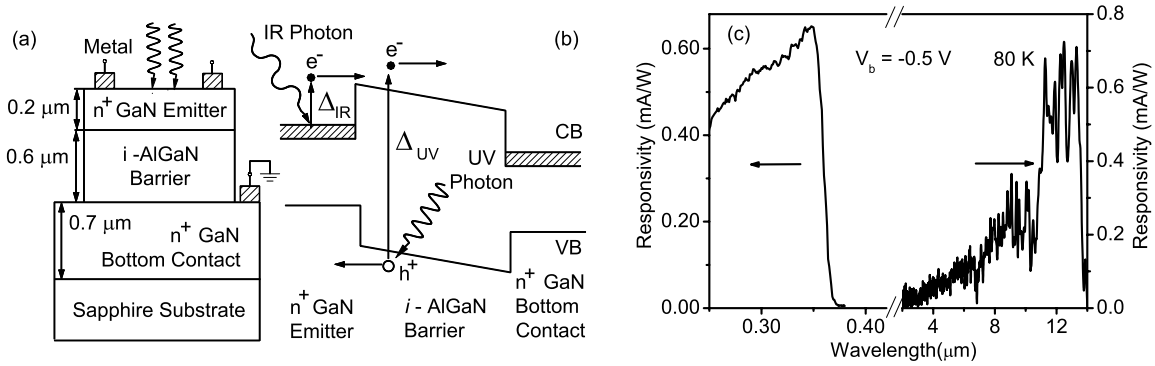

Figure 1. (a) The schematic diagram of GaN/AlGaN HEIWIP structure. The emitter (top contact) and the bottom contact are doped to $5\times10^{18}\mathrm{cm}^{-3}$ with Si as the n-type dopant, while the $Al_{0.026}Ga_{0.974}N$ barrier is not intentionally doped. (b) The band diagram showing the conduction/valence band (CB/VB) profile of the structure and the transitions leading to UV and IR responses. (c) The UV and IR response measured from the dualband detector.

the transitions for both mechanisms indicated is shown in Fig. 1(b) The UV detection is based on interband transitions of carriers in the AlGaN barrier. The threshold wavelength for the interband transition is given in nm by $\lambda_0^{UV} = 1240/E_g$ where E_g(eV) is the bandgap of the barrier layer. The IR detection is due to intraband transitions in the GaN (or AlGaN) emitter, and involves free carrier absorption, followed by the internal photoemission of photoexcited carriers across the junction barrier, and then the collection of carriers at the contacts due to the applied electric field . The offset between the Fermi level in the emitter layer and the conduction band edge of the barrier layer defines the interfacial workfunction (Δ), which arises due to the band offset of different materials,[13] and the band gap narrowing[14] of the highly doped emitter layer. The threshold wavelength λ_0^{IR} (in μm) is given by $1240/\Delta$, where Δ is in meV.

A useful property of these detectors is the thresholds for the UV and IR responses can be tailored separately by using AlGaN for both the emitter and barrier layers. The UV threshold is determined by the Al fraction in the barriers, and the IR threshold is determined by the difference in the Al fraction between the emitters and barriers. Thus, by adjusting the Al fraction in the barrier the desired UV threshold can be obtained; adjusting the Al fraction in the emitter allows the IR threshold to be tailored without changing the UV threshold. Previous work[12,15] on detectors using this design with GaN emitters and $Al_xGa_{1-x}N$ barriers shows an IR threshold shift from 15 to 8 μm as x is increased from 0.026 to 0.10.

The single barrier detectors described above have the ability to measure either UV and/or IR radiation while both radiations are incident on the detector. The two contacts do not allow direct separation of the currents from the two types of radiation, and distinguishing them will require separate modulation of the two radiation components. Initial tests measured the UV or IR spectra while the detector was exposed to a constant intensity of the other radiation (i.e., UV spectrum with constant IR, or IR spectrum with constant UV). The experimental setups and results are shown in Fig. 2 for UV and in Fig. 3 for IR radiation. The spectra show that IR radiation has negligible effect on the UV response, and the presence of UV radiation has only a very small effect on the IR response.

Measurements were also obtained with both the UV and IR signals chopped at different frequencies using the experimental setup in Fig. 4. This setup gave truely simultaneous measurements of the response, although the requirements for chopping at separate frequencies in order to distinguish the current components would place restrictions on practical applications. To avoid these complications more advanced designs have been developed in which the current components can be separated without resorting to separate modulation of the incident radiation.

The detector's top contact thickness was similar to the expected skin depth (0.1-0.2 μm) and hence was expected to absorb a significant fraction of the incident UV radiation without generating any response. Studies

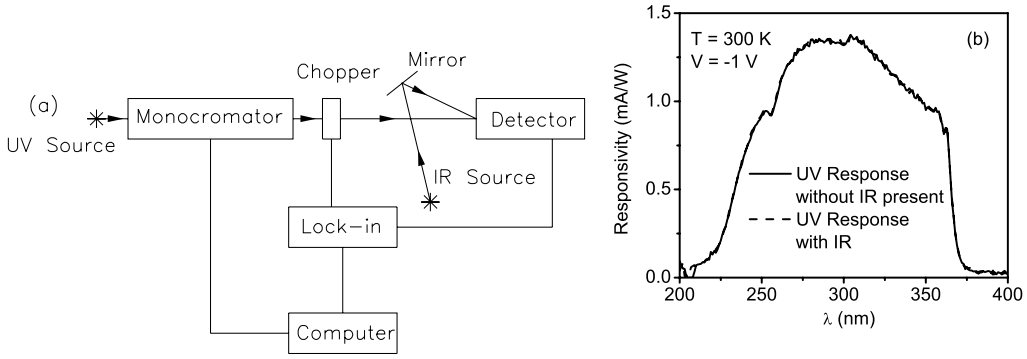

Figure 2. (a) The experimental setup for measuring UV response using a monochromator and a chopper both with and without IR radiation incident on the detector. (b) The UV response measured using a monochromator and a chopper both with and without IR radiation incident on the detector.

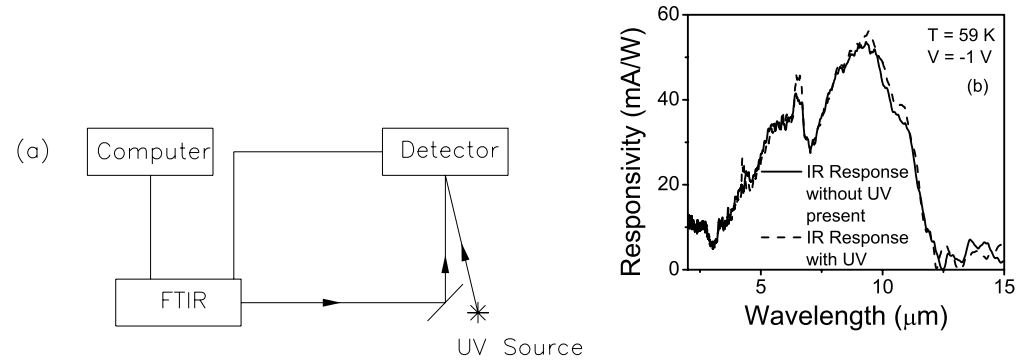

Figure 3. (a) The experimental setup for measuring IR response using an FTIR system both without and with UV radiation incident on the detector. (b) The IR response measured using an FTIR system both with and without UV radiation incident on the detector.

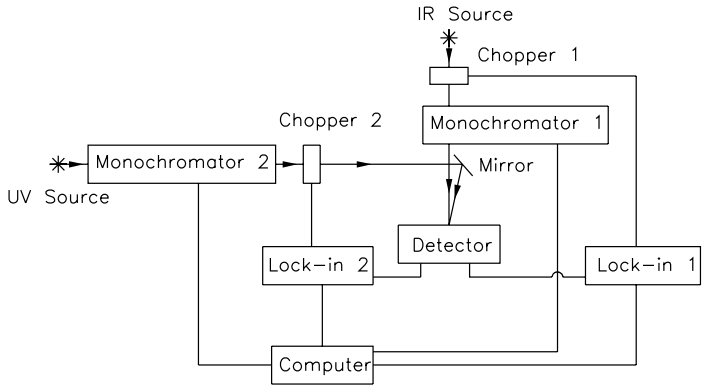

Figure 4. The experimental setup for measuring UV and IR responses simultaneously using two monochromator with separate choppers running at different frequencies. The different modulation frequencies allowed the two responses to be separated using the lock-in amplifiers.

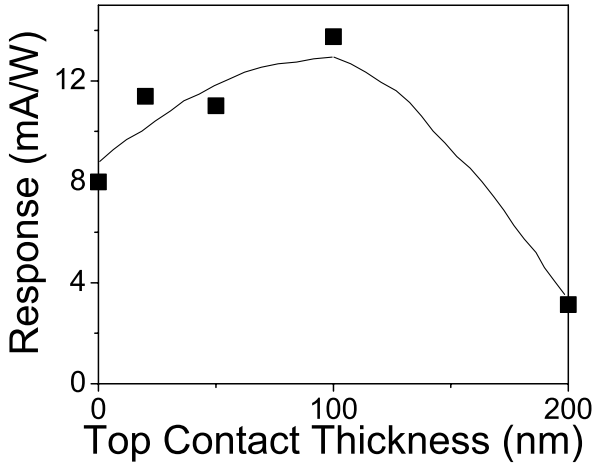

Figure 5. The change in the peak UV response when the top contact layer was etched to reduce its thickness. The optimal thickness was ~ 0.1 μm. The line is to guide the eye.

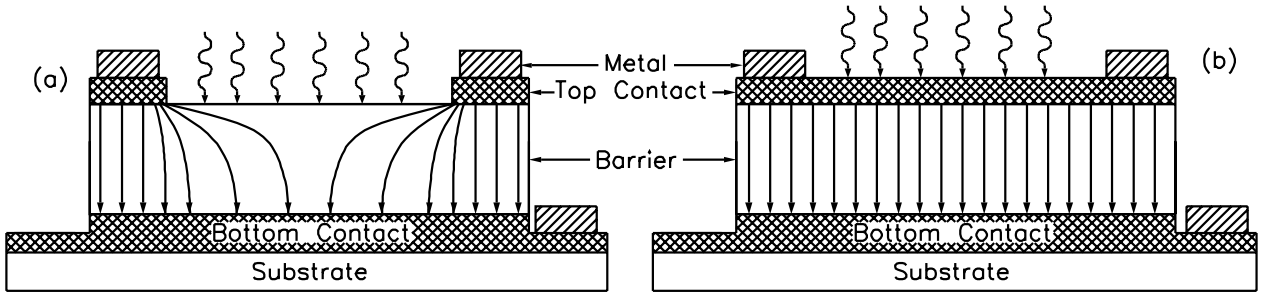

Figure 6. The distribution of the electric field in the barrier (a) with the top contact etched away and (b) without etching the top contact. The reduced field in (a) will lead to slower transport and hence more recombination of the electron-hole pairs.

were conducted on the effects of thining the top contact by etching to reduce the UV absorption in the contact improving the total UV response. The results for the peak UV responsivity with the top contact thickness are shown in Fig. 5. Although etching away the top contact improved the response slightly, it did not lead to as large an improvement as was expected. This is believed to be due to the effects of the electric field spreading. Therefore there was a need for a thin conducting layer to achieve a uniform electric field in the barrier region. A plot showing the electric field in the barrier both with and without the top contact layer is given in Fig. 6. The field near the center of the detector is reduced by a factor of nearly 100, which leads to a much slower carrier transport and an enhanced recombination of the electron-hole pairs. It was found that the optimal thickness for the top contact is ~ 0.1 μm in order to provide the required electric field in the barrier region.

Capacitance-voltage (C-V) measurements were carried out to look for the presence of traps in the single barrier sample. The results at different frequencies are shown in Fig. 7. The key feature is the presence of negative capacitance[16] for negative bias which can be related to traps at the emitter barrier interface. The traps should only be present at one interface due to the asymmetry of the C-V curve.

3. SIMULTANEOUS UV-IR DETECTOR

The simultaneous dual band detector design has separate UV and IR active regions and uses three contacts to separately measure the UV and IR photocurrents. This separation is possible due to the much higher UV absorption coefficient than for the IR range, and IR absorption only taking place in the highly doped emitter and

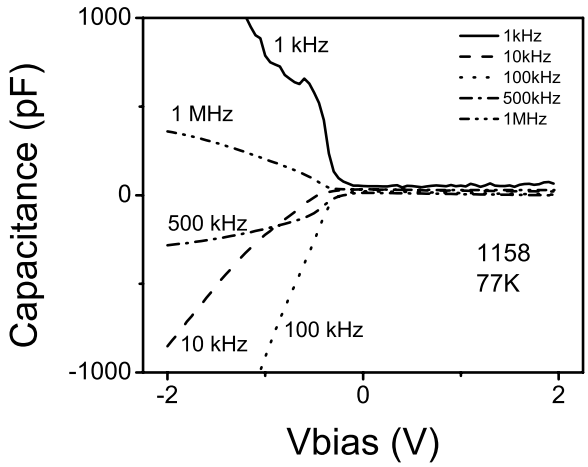

Figure 7. The capacitance-voltage measured for the sample at different frequencies for 77 K. The negative capacitance indicates the possible presence of traps at the emitter barrier interface.

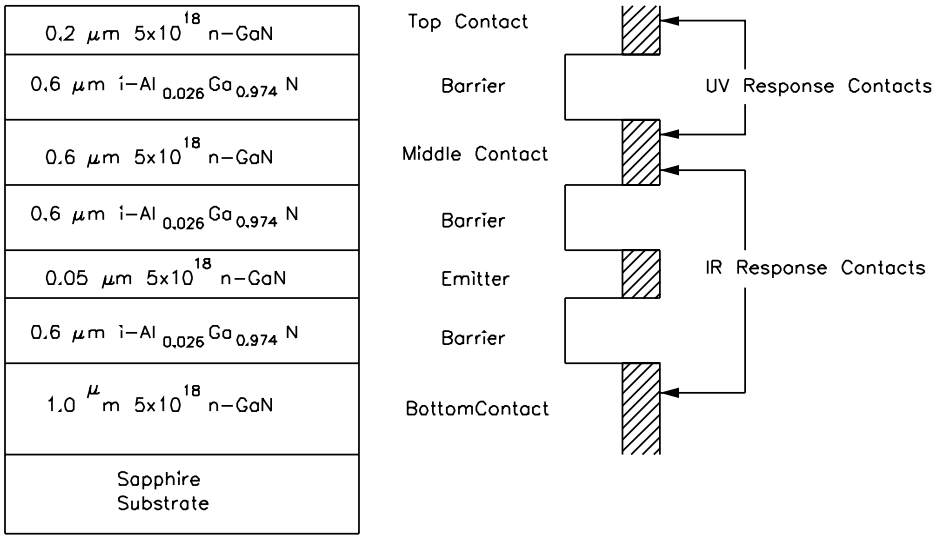

Figure 8. The three terminal structure for the simultaneous dual band response measurements showing separate regions and contacts for UV and IR measurements

contact regions. The design from the top down consists of the top contact, the UV active region, a middle contact, the IR active region, the bottom contact and the substrate. The UV active region consists of a single undoped AlGaN barrier. The IR response from the UV active region can be reduced to negligible values by etching the top contact down to the minimal thickness required to spread the electric field uniformly across the detector. For optimum operation the UV active region should be sufficiently thick ($\sim 1.2\ \mu$m) so that the UV radiation is completely absorbed before it reaches the IR active region. The IR active region will then respond only to the IR radiation. The UV response can be obtained by measuring the current between the top and middle contacts, and the IR response can be obtained by measuring the response between the middle and bottom contacts. Even if the IR response is not completely eliminated from the UV region and the UV response from the IR region, it should be possible to use the two measured currents to distinguish the UV and IR components which will be discussed later.

The design for the simultaneous UV-IR dual band detector structure is shown in Fig. 8. The three contacts

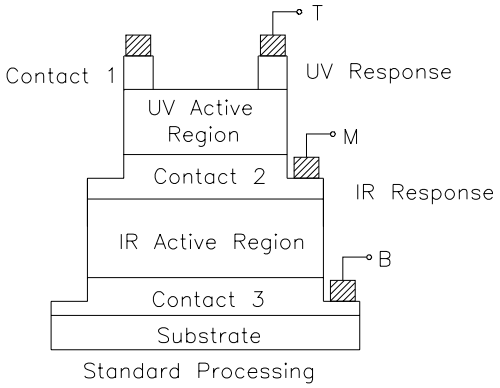

Figure 9. The processed structure for the simultaneous dual band response measurements with three contacts allowing separate readout of the UV and IR active regions. The labels T, M, and B will be used to indicate the top, middle and bottom connections(contacts 1, 2, and 3, respectively) for the following measurements.

allow separate biasing and measurement of the UV and IR active regions. The UV-IR dual band structure was grown by organometallic chemical vapor deposition (OMCVD) on sapphire substrate. The detector samples were processed by etching mesa detectors and depositing Ti/Al/Ti/Au [300/800/1200/550 Å] contacts. The etching and contacts were deposited so that connections could be made to all three contacts as shown in Fig. 9.

The UV and IR spectra were obtained separately for both active regions as shown in Figs. 10 and 11. Throughout the following discussion, the middle terminal will be common and positive bias will mean that the top or the bottom terminal is positive relative to the middle terminal. During the simultaneous measurements both active regions will be biased negatively so that the majority carriers move toward the middle contact. This will prevent photocarriers from crossing from one active region into the other, while at the same time giving minimum IR response in the UV active region.

For the IR active region, the UV response is reduced by 40% but not to near zero as was expected. Some of this effect may be due to the presence of a schottky contact at the top. This is further supported by the much stronger exciton peak observed for the IR active region (TM contacts) when compared to the broader response. If the exciton peaks are assumed to be equal for the two regions, the relative UV response from the IR region would be reduced to 10%. Increased thickness in the UV active region should reduce the UV response from the IR active region. For example, increasing the UV region barrier thickness from 0.6 to 1.2 μm reduces the UV response in the IR active region from 10% to 1%.

IR responses at 4.2 K are shown in Fig. 11. The UV active region did not show a measurable IR response under negative bias, but did show a response under positive bias as expected. The IR active region showed similar response under both bias directions. There are four different potential combinations for biasing the UV and IR active regions. However, the UV active region should be biased negatively in order to minimize IR response from the UV active region. Once the bias of the UV active region is determined, the IR active region should be biased in the same way (negatively) to prevent photocarriers from crossing between the two active regions.

For an ideal detector, the UV response should be obtained solely from the UV active region, and the IR response from the IR active region. The schottky top contact reduced the accuracy of calibration for a current signal so the results were left as voltage signals for fixed load values. The voltage response can be used to identify the signal, and would only vary from the current signal by a constant factor for constant loads. Wavelengths of 340 nm for the UV and 9.3 μm for the IR ranges were chosen for intensity tests. In these tests the wavelengths were held constant, while the combination of incident radiation was varied. A single chopper, as shown in Fig. 12, was used for both the UV and IR radiations. Both radiations had the same modulation as would be the case in a typical application. The measured signals from the UV and IR active regions were averaged over a period of 30 seconds for different combinations of incident radiation and are given in Table 1. The UV active region showed no IR signal and can therefore be used directly to determine the UV intensity. However, because the UV active region was not thick enough to block all the UV radiation, there was still a UV response in the IR active

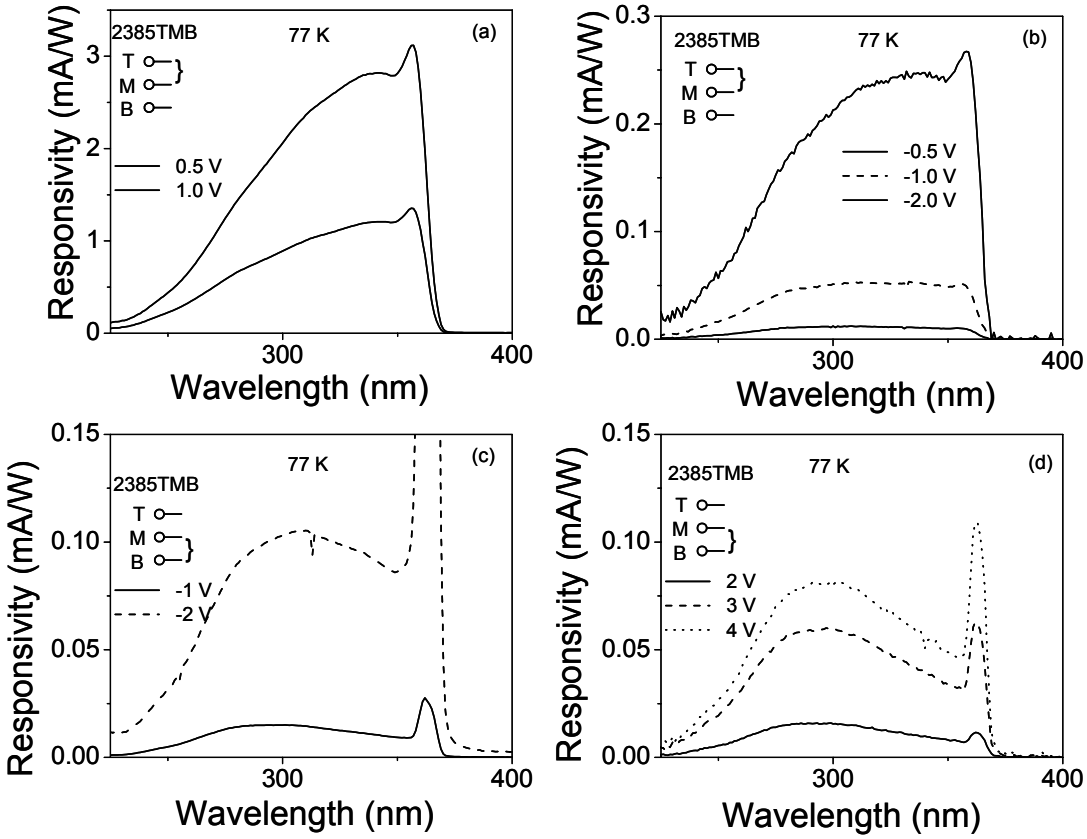

Figure 10. The UV response of sample 2385TMB for the UV active region under (a) forward and (b) reverse bias at 77 K. The UV response for the IR active region under (c) reverse and (d) forward bias at 77 K. Although expected to be zero, the UV response from the IR active region (MB contacts) was 40% of the response from the UV active region (TM contacts).

region. Increasing the UV active region to 1.2 μm should reduce the UV response in the IR active region to negligible values. This will allow direct, simultaneous measurement of the two components without requiring any calculations. However, for this sample the change in response from the IR region when IR radiation is applied can be observed indicating the dual band response.

In order to obtain as much information as possible from the present sample, an approach was developed to separate the UV and IR signals. To determine the UV and IR response, the fractions of the response from each region were determined from measurements using only UV or IR radiation as follows

$$f = \frac{R_{UV,1}}{R_{UV,1} + R_{UV,2}} \tag{1}$$

$$g = \frac{R_{IR,1}}{R_{IR,1} + R_{IR,2}} \tag{2}$$

where the subscripts UV and IR on the response R refer to the UV and IR incident radiation respectively, and the subscripts 1, 2 refer to the top (UV active) and bottom (IR active) regions of the detector respectively. Using these fractions the total IR and UV responses are then given by

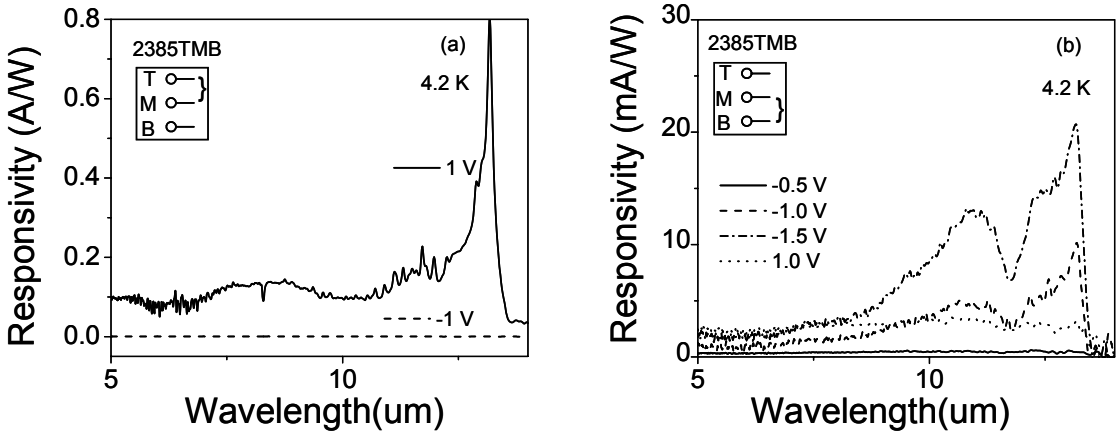

Figure 11. The IR response from (a) the UV active region and (b) the IR active region of sample 2385TMB measured at 4.2 K. The UV active region showed IR no response from the top contact under negative bias as desired, and had response from the middle contact under positive bias as expected. The IR active region showed IR response for both bias directions and with similar response.

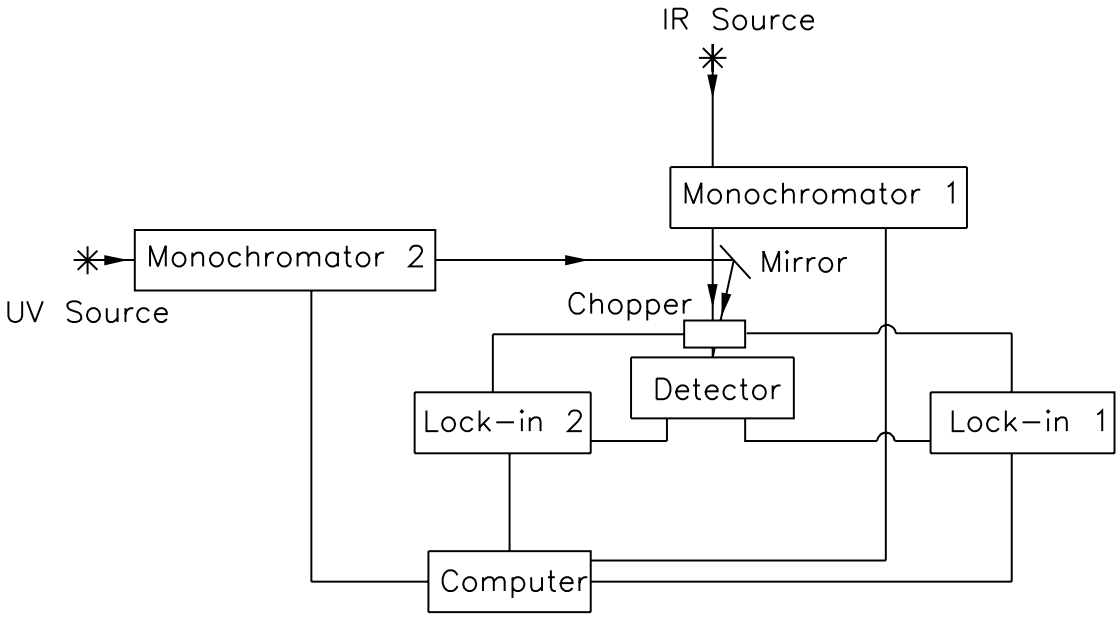

Figure 12. The experimental setup for measuring the UV and IR components simultaneously using a single chopper. The two lockin amplifiers will measure the response from the UV and IR active regions respectively, giving the desired dualband response.

Table 1. The observed response in the UV and IR active regions for different combinations of IR and UV radiation. The radiation was reduced from its maximum value by use of filters and is given as a fraction of the maximum.

UV ACTIVE REGION		
	With UV	Without UV
With IR	0.36 mV	0.00 mV
Without IR	0.36 mV	0.00 mV
IR ACTIVE REGION		
	With UV	Without UV
With IR	0.67 mV	0.22 mV
Without IR	0.25 mV	0.00 mV

$$R_{IR} = \frac{(1-f)R_1 - fR_2}{f-g} \tag{3}$$

$$R_{IR} = \frac{(1-g)R_1 - gR_2}{g-f} \tag{4}$$

where R_1 and R_2 are the measured responses from the top and bottom regions respectively.

4. CONCLUSIONS

Results have been presented showing dual band UV-IR response in a GaN/AlGaN detector. The response does not require separate modulation of the incoming light in the two ranges and both ranges can be measured simultaneously. This approach can be applied on other materials in order to expand to other wavelength range combinations. For example, a GaAs/AlGaAs detector could be designed to cover the NIR and FIR ranges.

ACKNOWLEDGMENTS

This work was supported in part by the US Air Force Small Business Innovation Research (SBIR) under Grant FA9453-05-M-0106.

REFERENCES

1. M. A. Khan, J. N. Kuznia, D. T. Olson, M. Blasingame, and A. R. Bhattarai, "Schottky barrier photodetector based on Mg-doped p-type GaN films", *Appl. Phys. Lett.* **63**, pp. 2455-2456, 1993.
2. D. Walker, X. Zhang, P. Kung, A. Saxler, S. Javadpour, J. Xu, and M. Razeghi,"AlGaN ultraviolet photoconductors grown on sapphire", *Appl. Phys. Lett.* **68**, pp. 2100-2101, 1996.
3. M. Furis, A. N. Cartwright, H. Wu, and W. J. Schaff, "Room-temperature ultraviolet emission from GaN/AlN multiple-quantum-well heterostructures", *Appl. Phys. Lett.* **83**, pp. 3486-3488, 2003.
4. S. K. Zhang, W. B. Wang, I. Shtau, F. Yun, L. He, H. Morkoc, X. Zhou, M. Tamargo, and R. R. Alfano, "Back-illuminated GaN/AlGaN heterojunction ultraviolet photodetector with high internal gain", *Appl. Phys. Lett.* **81**, pp. 4862-4864, 2002.
5. J. P. Zhang, X. Hu, Yu. Bilenko, J. Deng, A. Lunev, M. S. Shur, R. Gaska, M. Shatalov, J. W. Yang, and M. A. Khan, "AlGaN-based 280 nm light-emitting diodes with continuous-wave power exceeding 1 mW at 25 mA", *Appl. Phys. Lett.* **85**, pp. 5532-5534, 2004.
6. V. D. Jovanovic, D. Indjin, Z. Ikonic, and P. Harrison, "Simulation and design of GaN/AlGaN far-infrared ($\lambda \sim 34$ μm) quantum-cascade laser", *Appl. Phys. Lett.* **84**, pp. 2995-2997, 2004.
7. C. Gmachl, H. M. Ng, and A. Y. Cho, "Intersubband absorption in GaN/AlGaN multiple quantum wells in the wavelength range of $\lambda \sim 1.75$ - 4.2 μm", *Appl. Phys. Lett.* **77**, pp. 334-336, 2000.

8. N. Biyikli, T. Kartaloglu, O. Aytur, I. Kimukin, and E. Ozbay, "Solar-blind AlGaN-based Schottky photodiodes with low noise and high detectivity", *Appl. Phys. Lett.* **81**, pp. 3272-3274, 2002.
9. A. Goldberg, P. N. Uppal, and M. Winn, "Detection of buried land mines using a dual-band LWIR/LWIR QWIP focal plane array", *Infrared Physics & Technology* **44**, pp. 427-437, 2003.
10. H. C. Liu, C. Y. Song, A. Shen, M. Gao, Z. R. Wasilewski, and M. Buchanan, "GaAs/AlGaAs quantum-well photodetector for visible and middle infrared dual-band detection", *Appl. Phys. Lett.* **77**, pp. 2437-2439, 2000.
11. M. P. Touse, G. Karunasiri, K. R. Lantz, H. Li, and T. Mei, "Near- and mid-infrared detection using $GaAs/In_xGa_{1-x}As/In_yGa_{1-y}As$ multiple step quantum wells", *Appl. Phys. Lett.* **86**, pp. 093501, 2005.
12. G. Ariyawansa, M. B. M. Rinzan, M. Alevli, M. Strassburg, N. Dietz , A. G. U. Perera, S. G. Matsik, A. Asghar, I. T. Ferguson, H. Luo, A. Bezinger, and H. C. Liu, "GaN/AlGaN ultraviolet/infrared dual-band detector", *Appl. Phys. Lett.* **89**, pp. 091113, 2006.
13. D. G. Esaev, M. B. M. Rinzan, S. G. Matsik, and A. G. U. Perera, "Design and optimization of GaAs/AlGaAs heterojunction infrared detectors", *J. Appl. Phys.* **96**, pp. 4588-4597, 2004.
14. W. Z. Shen, A. G. U. Perera, H. C. Liu, M. Buchanan, and W. J. Schaff, "Bias effects in high performance GaAs homojunction far-infrared detectors", *Appl. Phys. Lett.* **71**, pp. 2677-2679, 1997.
15. A. G. U. Perera, G. Ariyawansa, M. B. M. Rinzan, M. Stevens, M. Alevli, N. Dietz, S.G. Matsik, A. Asghar, I.T. Ferguson, H. Luo, A. Bezinger, and H. C. Liu, "Performance improvements of ultraviolet/infrared dual-band detectors", *Infrared Physics & Technology* **50**, pp. 142-148 2007.
16. A. G. U. Perera, W. Z. Shen, M. Ershov, H. C. Liu, M. Buchanan, and W. J. Schaff, "Negative capacitance of GaAs homojunction far-infrared detectors", *Appl. Phys. Lett.* **74**, pp. 3167-9, 1999.